ACS OMEGA

Open Access

http://pubs.acs.org/journal/acsodf

Article

Aluminum−Lithium Alloy Fillers Enhancing the Room Temperature Performances of Polymer Electrolytes for All-Solid-State Lithium Batteries

Dongyan Ren,*[,§] Xin Tang,[§] Qiqiang Wang, Haifeng Du, and Ling Ding

Cite This: *ACS Omega* 2024, 9, 35920−35928

Read Online

ACCESS | Metrics & More | Article Recommendations | Supporting Information

ABSTRACT: Poly(ethylene oxide) (PEO) electrolytes usually suffer from low room temperature (RT) ionic conductivity and a narrow voltage window, which limits the improvement of energy density and practical applications in all-solid-state batteries. Composite polymer electrolytes (CPEs) are regarded as the common method to reduce the crystallinity of polymers and increase the lithium ion conductivity. Compared with active or inert ceramic material fillers in previous studies, aluminum−lithium alloy fillers are used to prepare composite electrolytes in this study, showing excellent performance at room temperature. The conductivity of the PEO-based electrolytes increases by a factor of 3.62−3.62× 10^{-4} S cm^{-1} at RT with 5 wt % Al−Li alloy. The transference number of Li^+ is increased to 0.524. The characteristics of the Al−Li alloy and higher conductivity enable the composite electrolyte to stabilize the interface with the electrodes, reducing the polarization of solid-state batteries. The all-solid-state Li/PEO-5%/$LiFePO_4$ cells show the highest initial discharge capacity of 153 mAh g^{-1} and the highest stable discharge capacity of 147 mAh g^{-1} with the initial Coulombic efficiency of more than 100%. It also exhibits the best rate capacity and cycle performance (90% capacity retention rate after 100 cycles).

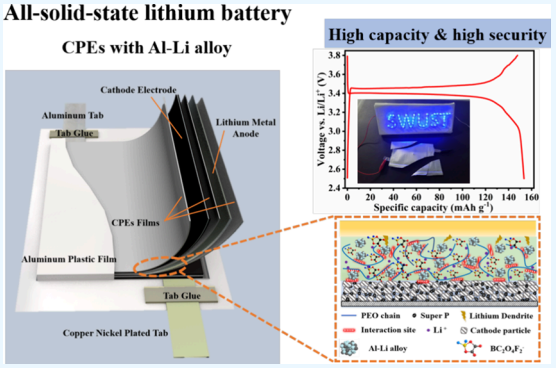

1. INTRODUCTION

Lithium-ion batteries (LIBs) have achieved tremendous success as one of the energy-storage systems, and the demand for energy density is ever-increasing, especially in major participating countries.[1−3] With the advantage of high theoretical capacity (3860 mAh g^{-1}) and the lowest potential (−3.04 V vs H^+/H_2), the Li-metal anode can greatly improve the energy density.[4] However, the growth of lithium dendrites in liquid electrolytes has always been a thorny problem.[5] Furthermore, the safety performance and energy density of LIBs are also limited by organic liquid electrolytes due to their flammable property and intrinsic narrow electrochemical window.[6,7] As one of the effective solutions, solid-state electrolytes (SSEs) in all-solid-state lithium batteries (ASLIBs) have been studied extensively to replace organic liquid electrolytes.[8]

Among the solid inorganic electrolytes (SIEs), in addition to LiPON, Li_3N, and halide, the best representatives are oxide electrolytes [e.g., garnet-type electrolyte $Li_xLa_3Zr_2O_{12}$ (LLZO) or $Li_{6.4}La_3Zr_{1.4}Ta_{0.6}O_{12}$ (LLZTO), NASICON-type electrolyte $Li_{1.3}Al_{0.3}Ti_{1.7}(PO_4)_3$ (LATP) or $Li_{1.5}Al_{0.5}Ge_{1.5}(PO_4)_3$ (LAGP), perovskite-type electrolyte $Li_{0.33}La_{0.557}TiO_3$ (LLTO), etc.] and sulfides (e.g., Li_3PS_4, $Li_7P_3S_{11}$, $Li_{10}GeP_2S_{12}$, etc.). Even with high mechanical strength and ionic conductivity, the huge interfacial impedance hinders the transport of Li^+ at the interfaces between electrodes and solid electrolytes.[9] Furthermore, the penetration of lithium dendrite along grain boundaries in garnet-type electrolytes and the instability of LAGP or LATP to lithium metal as well as the fragility of ceramics all limit the application of oxide electrolytes in ASLIBs.[10−12] Although sulfide has the highest ionic conductivity, its high sensitivity to air and water, poor stability at low potentials, and huge volume changes during lithium deposition and dissolution hinder its application in ASLIBs.[13,14] Among the solid polymer electrolytes (SPEs), poly(acrylonitrile) (PAN), poly(methyl methacrylate) (PMMA), and poly(vinylidene fluoride) (PVDF) are more commonly applied to solid gel electrolytes. Poly(ethylene oxide) (PEO) is a better complexing agent for Li^+ due to its lower glass transition temperature (T_g: approximately −64 °C) compared with other polymers, so PEO has been studied most extensively among ASLIBs.[6] The flexibility and workability of SPEs can solve the interface problems of ASLIBs, but their

Received: May 29, 2024
Revised: July 7, 2024
Accepted: July 18, 2024
Published: August 6, 2024

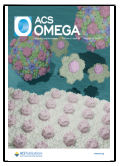

Table 1. PEO-Based Composite Polymer Electrolytes with Inorganic Fillers

inorganic filler	geometry	filler content	Li salt	ionic conductivity (S cm^{-1})	temperature (°C)
Al_2O_3[23]	microparticles	17.5 wt %	LiFSI	4.8×10^{-6}	RT
$MgAl_2O_4$[16]	microparticles	10 wt %	$LiPF_6$	2×10^{-5}	60
SiO_2[24]	mesoporous particle	7.5 wt %	$LiClO_4$	$\approx 10^{-4}$	50
ZrO_2[17]	nanoparticle	10 wt %	$LiBF_4$	2×10^{-4}	60
TiO_2[18]	nanoparticle	10 wt %	$LiClO_4$	$\approx 10^{-5}$	30
$LiAlO_2$[19]	nanoparticle	9 mol %	$LiClO_4$	9.8×10^{-5}	RT
MOF-5[20]	nanoparticle	10 wt %	LiTFSI	3.2×10^{-5}	RT
$BaTiO_3$[25]	nanoparticle	10 wt %	LiTFSI	5.2×10^{-3}	80
$Li_{0.33}La_{0.56}TiO_3$[26]	nanoparticle	10 wt %	$LiClO_4$	2.8×10^{-3}	65
$Li_{1.3}Al_{0.3}Ti_{1.7}(PO_4)_3$[27]	nanoparticle	50 wt %	$LiClO_4$	1.6×10^{-5}	80
$Li_{0.33}La_{0.557}TiO_3$[28]	nanowires	15 wt %	LiTFSI	2.4×10^{-4}	RT
$Li_{1+x}Al_xTi_{2-x}(PO_4)_3$[29]	nanowires	40 vol %	$LiClO_4$	5.2×10^{-5}	RT
$Li_{6.28}La_3Al_{0.24}Zr_2O_{12}$[22]	nanowires	70 wt %	LiTFSI	4.9×10^{-4}	RT
$Li_{0.33}La_{0.557}TiO_3$[30]	nanowires	5 wt %	LiTFSI	5.5×10^{-4}	RT
$Li_{1.3}Al_{0.3}Ti_{1.7}(PO_4)_3$[31]	compact layer	70 wt %	LiTFSI	2.5×10^{-4}	60
$Li_{0.3}La_{0.557}TiO_3$[32]	3D networks	~20 wt %	LiTFSI	1.8×10^{-4}	RT
2 LATP/PAN[33]	3D networks	30 wt %	LiTFSI	6.5×10^{-4}	60
$Li_{6.28}La_3Zr_2Al_{0.24}O_{12}$[34]	3D networks	20.7 wt %	$LiClO_4$	2.3×10^{-5}	30
$Li_7La_3Zr_2O_{12}$[35]	3D networks	/	LiTFSI	1.2×10^{-4}	RT
LICGC[36]	3D networks	77 wt %	LiTFSI	3.5×10^{-5}	20
$Li_{10}GeP_2S_{12}$[37]	powders	1 wt %	LiTFSI	1.2×10^{-3}	80
$Li_{10}SnP_2S_{12}$[38]	powders	1 wt %	LiTFSI	1.7×10^{-4}	55

extremely low conductivity at room temperature is an inherent defect. Compared with simple modification methods such as doping, coating, cross-linking, copolymerization, and blending, using composite polymer electrolytes (CPEs) is obviously a more feasible method to prepare high energy density and high safety batteries.[15]

The studies of PEO-based CPEs in recent years are listed in Table 1. The fillers are divided into inert fillers (e.g., Al_2O_3, SiO_2, TiO_2, $BaTiO_3$, etc.) and active fillers (e.g., LLTO, LLZO, LATP, LAGP, $Li_{10}GeP_2S_{12}$, etc.). Firstly, the crystallinity of PEO at room temperature can be significantly reduced by inorganic fillers, which enhances the transfer of Li^+ on the ether oxygen group of the PEO molecular chain segment.[16−19] Secondly, inorganic fillers can promote the dissociation of lithium salts in electrolytes, improving the concentration and mobility of active lithium ions through Lewis acid−base interactions.[20−22] Thirdly, the active fillers can also provide additional amounts and transmission paths of Li^+.

However, there are still several problems in CPE studies. First, for some CPEs containing inorganic fillers with poor stability to lithium metal (e.g., LATP, LAGP, or $Li_{10}GeP_2S_{12}$, etc.), the electronic conductivity will be introduced when in contact with the lithium metal anode due to the reduction action of inorganic fillers, reducing the practical Li^+ transference number. Second, the majority of fillers in Table 1 contain many valuable metals such as Ti, La, Zr, Ta, Ge, and more, and the processes of ceramic calcining (especially with special morphology) and sulfide grinding are both complicated and time-consuming, which makes the cost of CPEs increase obviously. Third, the room temperature conductivity of some CPEs cannot meet the actual use requirements of ASLIBs. Therefore, it is necessary to develop a composite polymer electrolyte that has stability to lithium metal, good room temperature conductivity, ideal cost advantage, and good operability for the large-scale application of ASLIBs.

In this study, we designed a kind of PEO-based CPE that contains Al−Li alloy to improve the conductivity of the polymer electrolyte and the electrochemical performance of ASLIBs. As a direct Li^+ conductor, Al−Li alloy has not only the advantages of simple preparation and low cost, but also a much higher conductivity than other inorganic fillers, which means that a smaller added amount of Al−Li alloy can get the desired effect. In addition to improving the ionic conductivity and Li^+ migration number of the polymer electrolyte at room temperature, the Al−Li alloy can also stabilize the interface, reduce polarization, compensate capacity fading, increase Coulombic efficiency, and improve cycle performance in ASLIBs. The experimental results show that the addition of Al−Li alloy can significantly improve the performance of ASLIBs at room temperature, especially in terms of maintaining high capacity and better rates, which can further prove that the CPEs containing Al−Li alloy have broad application prospects.

2. EXPERIMENTAL SECTION

2.1. Synthesis of Al−Li Alloy. The lithium foil and aluminum foil were stacked together at less than 3% relative humidity with the weight ratio of Al/Li (Li: Al = 1:1.5). After mechanical disruption, the mixture was heated at 180 °C for 5 h in argon to melt lithium metal and then was calcined at 680 °C for 5 h to obtain a homogeneous Al−Li alloy. The ball-milled alloy powder is used as a filler for the CPEs.

2.2. Preparation of CPEs and All-Solid-State Batteries. The dried PEO (M_w ~ 600,000) and dried lithium difluoro(oxalato)borate (LiDFOB) were dissolved into N, N-dimethylformamide (DMF) with the equivalent molar ratio (EO/Li^+ = 20), stirring at 60 °C for 8 h to obtain a homogeneous viscous liquid. Then the Al−Li alloy powder with different weight ratios (5, 7.5, and 10 wt %) was added to the previous solution. After stirring at 55 °C for 24 h, the uniform suspension was cast onto a Teflon plate and then dried at 80 °C in vacuum for 48 h to remove DMF. The all-solid-state battery is composed of a cathode electrode, a CPE membrane, and a lithium metal foil. The cathode consists of 80

https://doi.org/10.1021/acsomega.4c05040
ACS Omega 2024, 9, 35920−35928

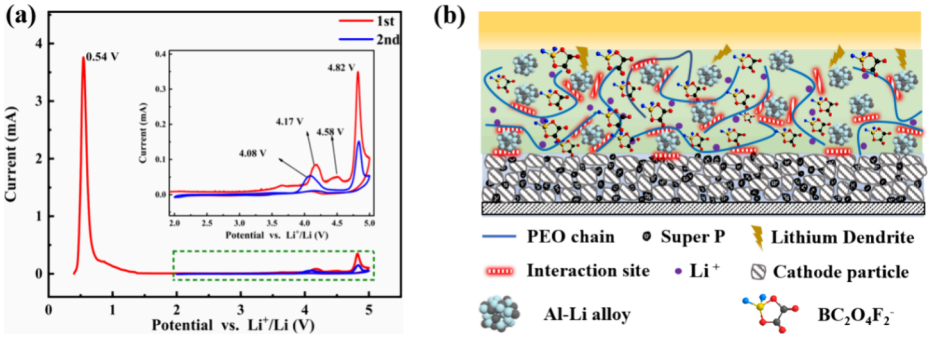

Figure 1. (a) CV curve of Al−Li alloy. (b) Schematic diagram of the electrolyte interaction between lithium metal and the cathode electrode.

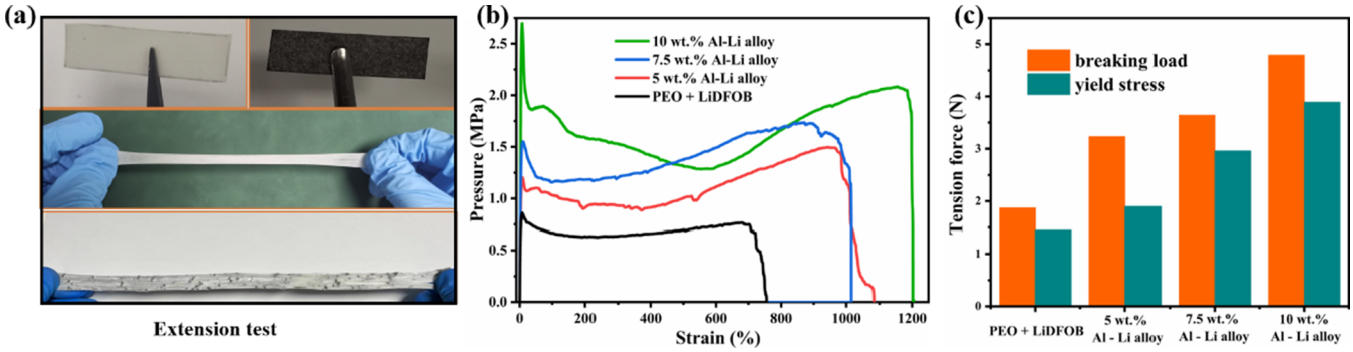

Figure 2. Mechanical property test results of CPE membranes (a) the physical map, (b) stress−strain curves, and (c) comparison diagram of yield and fracture strength.

wt % $LiFePO_4$, 12 wt % PEO, 5 wt % super P carbon black, and 3 wt % LiDFOB.

2.3. Characterization and Measurement. An X-ray diffractometer (XRD, DMAX1400 Rigaku) and a field emission scanning electron microscope (FSEM, UItra55) were used for phase identification and morphology examination. The thermal performance was analyzed using thermal gravity analysis and a differential scanning calorimeter (TG-DSC, SDT Q160). The mechanical properties of CPE membranes (1 cm × 4 cm) were measured using a universal testing machine (UTM-4000, SUNS, Shenzhen) with a stretching speed of 1.5 mm s^{-1}. Fourier transform infrared (FT-IR, Nicole-5700) was utilized to probe the structure changes in the wave region of 4000−400 cm^{-1}.

The room ionic conductivity of CPEs was measured by electrochemical impedance spectroscopy (EIS) of CR2032 cells in which the CPEs were sandwiched between two stainless-steel (SS) blocking electrodes over the frequency range from 10^{-1} to 10^{6} Hz with an applied voltage of 5 mV. The lithium-ion transference numbers (t_{Li}^{+}) were measured by a combination of EIS and amperometric I−t curves using Li|SPE|Li symmetric cells. The electrochemical stability windows of CPEs were analyzed by linear sweep voltammetry (LSV) using Li|SPEs|SS cells with a scanning rate of 1 mV s^{-1} from 2.5 to 6 V (vs Li/Li^{+}). The cyclic voltammetry (CV) was tested in 0−5 V with a scanning rate of 0.1 mV s^{-1}. The above measurement methods were all tested by an electrochemical workstation (CHI760, Chenhua, China) at room temperature. The battery performances of all-solid-state batteries (including coin cells and flexible packaging batteries) were tested by the NEWARE CT2001A battery test system (Wuhan, China) within the voltage range between 2.5 and 3.8 V.

3. RESULTS AND DISCUSSION

According to the XRD patterns of Al−Li alloys with different weight ratios (Figure S1), the main phase of Al−Li alloys is Al_4Li_9 (PDF#24-0008). However, as the weight proportion increases of aluminum foil, the intensity of the diffraction peak at 2θ = 40° also significantly increases, corresponding to the content increase of AlLi (PDF#03-1215). Therefore, the Al−Li alloy with the weight ratios of Li:Al = 1:1.5 was added as the filler into PEO polymer to avoid the influence of more impurities in alloys.[39] To investigate the intrinsic electrochemical characteristics of the Al−Li alloy, cyclic voltammetry was carried out. As shown in Figure 1a, the oxidation peak appears at 0.54 V at the scanning rate of 0.1 mV/s corresponding to the release of Li^{+}. Several slight oxidation peaks between 4 and 5 V correspond to the oxidation of Li_3N and Li_2O, respectively. Obviously, if the Al−Li alloy is used as the filler of PEO-based CPEs, Li^{+} will be released at a potential above 0.54 V to increase the concentration of lithium ions in CPEs and thus increase the conductivity. The schematic diagram in Figure 1b shows that the Al−Li alloy can not only release Li^{+}, but also improve the stability of CPEs to lithium and reduce the crystallinity of CPEs through interaction with the PEO molecular chain. The initial charge/discharge curves of Al−Li alloys (Figure S2) show the excellent ability of Al−Li alloys to release Li^{+}. The Al−Li alloy with the weight ratios of Li: Al = 1:1.5 exhibited the highest initial charge capacity of 963.5 mAh g^{-1}, but the initial discharge capacity of Al−Li alloys can be ignored, which is consistent with the CV results shown in Figure 1a. Moreover, due to the fast lithium kinetics of Al−Li alloy, Li^{+} can rapidly diffuse in Al−Li alloy fillers with 10^{-7} cm^2/s at room temperature.[40]

The mechanical property test results of CPE membranes are shown in Figure 2, and CPE membranes (1 cm × 4 cm) were

https://doi.org/10.1021/acsomega.4c05040
ACS Omega 2024, 9, 35920−35928

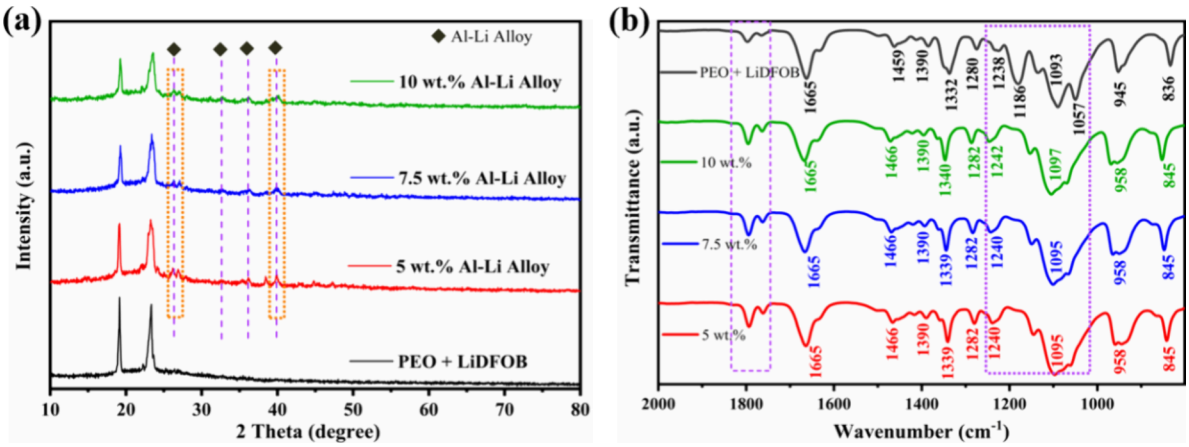

Figure 3. (a) XRD patterns of the pristine PEO + LiDFOB solid electrolyte and the CPEs with various Al−Li alloy contents. (b) FTIR spectra of the above four solid electrolytes.

stretched with a stretching speed of 1.5 mm s^{-1}. The maximum load, yield strength, and fracture strength of the membrane increase with the increasing amount of Al−Li alloy in the CPEs. Compared with solid electrolytes of pure PEO, CPEs containing Al−Li alloy have better mechanical properties and are more conducive to resisting the puncture of lithium dendrites. Figure S3 shows the resulting thermogravimetric curves, with decomposition temperatures above 350 °C for all materials, and it is worth noting that the lower Td values of PEO + LiDFOB membranes compared to CPEs membranes added to Al−Li alloy are attributed to their poor thermal stability.

Figure 3a shows the XRD patterns of 4 CPE membranes. Due to the crystalline property of PEO, there are two distinct sharp peaks at around 19.2° and 23.6° representing (120) and (112) planes, respectively. After the addition of the Al−Li alloy, the peak intensities of these two peaks were significantly weakened, indicating a decrease in the crystallinity degree of the PEO backbone caused by the demolition effect of the Al−Li alloy on the ordered arrangement of the PEO chains. Compared with PEO + LiDFOB, the XRD peaks at around 27° just correspond to the Al−Li alloy. Moreover, the oxidation products (Li_2CO_3 and Li_2O, etc.) were not observed in the XRD patterns.

To explore the effect of Al−Li alloy addition on the PEO matrix structure, FTIR spectra of PEO + LiDFOB and PEO + LiDFOB + Al−Li alloy are measured and shown in Figure 3b. Compared with the spectrum of the pristine PEO + LiDFOB solid electrolyte, there are three obvious differences in the spectra of the CPEse with the addition of the Al−Li alloy. First, upon the addition of Al−Li alloy, the adsorption peaks corresponding to the stretching mode of −C═O (found in cyclic anhydride with a five-membered ring structure) in LiDFOB, located within the wavenumber range of 1800−1750 cm^{-1}, exhibited enhanced intensity. This observation suggests that the interaction between the Al−Li alloy particles and the ether oxygen groups present in PEO facilitated the dissociation of the lithium salt. Second, in the spectrum of the pristine PEO + LiDFOB solid electrolyte, the three adsorption peaks at 1057, 1093, and 1186 cm^{-1} are all characteristic of C−O−C stretching mode, but only a peak around 1095 cm^{-1} remained after the addition of Al−Li alloy, which illustrates that Al−Li alloy particles can weaken the complexation of Li^+ with ether oxygen groups. Third, the four adsorption peaks at 945, 1238, 1280, and 1332 cm^{-1} corresponding to the CH_2 bending vibration mode shifted toward a higher wavenumber after the addition of Al−Li alloy, further indicating the attenuation of the complexation of Li^+ with ether oxygen groups. Because the ether oxygen group not only realizes the movement of Li^+ on the PEO segment through the breaking and formation of the Li−O bond, but also induces the CH_2 of the molecular segment and undergoes electron transfer due to its electronegativity. Therefore, when the bonding of the ether oxygen group to Li^+ is slightly weakened, the induction effect of oxygen electronegativity on CH_2 is further strengthened, resulting in the absorption peak of CH_2 moving to the high band.

Figure 4 shows the photographs and SEM images of the CPE membranes. The inclusion of the Al−Li alloy is shown to enhance the mechanical strength of the CPEs while preserving the flexibility inherent to polymer solid electrolytes. For the semitransparent PEO + LiDFOB electrolyte membrane, a porous and loose surface morphology can be observed from its SEM image. With the increase of Al−Li alloy addition, the color of the membranes gradually deepened and the alloy particles can fill the holes of the membranes. However, at a 10 wt % Al−Li alloy concentration, significant agglomeration of

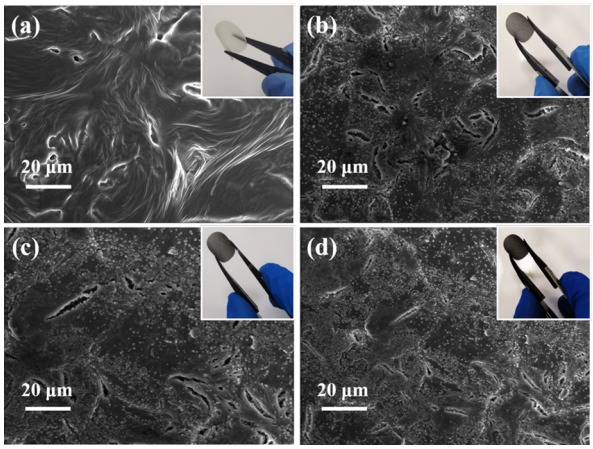

Figure 4. Photographs and SEM images of the (a) PEO + LiDFOB solid electrolyte membrane, (b) CPE membrane with 5 wt % Al−Li alloy, (c) CPE membrane with 7.5 wt % Al−Li alloy, and (d) CPE membrane with 10 wt % Al−Li alloy.

https://doi.org/10.1021/acsomega.4c05040
ACS Omega 2024, 9, 35920−35928

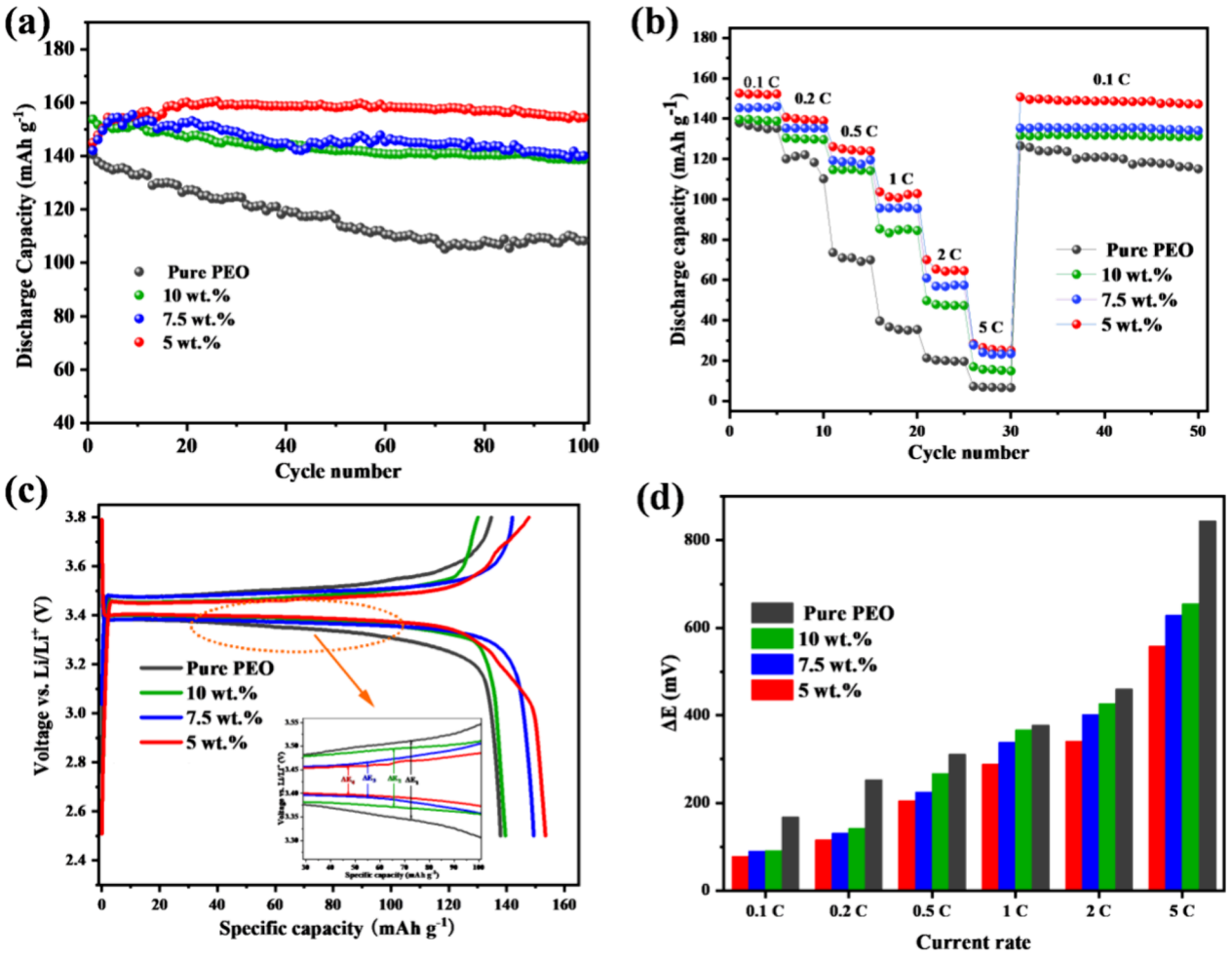

Figure 5. (a) Long cycle performance and (b) rate of the PEO + LiDFOB solid electrolyte and the CPEs with various Al−Li alloy contents. (c) Voltage−capacity curves of the PEO + LiDFOB solid electrolyte and the CPEs with various Al−Li alloy contents-based Li half batteries at 0.1 C. (d) Histogram of magnification potential difference.

alloy particles becomes evident within the CPE membrane. Such agglomerates, characterized by a larger particle size, not only fail to effectively reduce the crystallinity of the PEO solid electrolyte but also introduce a risk of short-circuiting within the battery. This occurs because the Al−Li alloy serves as a conductor for both lithium-ions and electrons.[40,41] Therefore, excessive addition of the alloy could facilitate direct electrical pathways between the cathode and anode electrodes, potentially compromising the integrity of the cell.

We conducted a systematic investigation into the cycling and rate performances of solid-state batteries assembled by pairing CPEs with $LiFePO_4$ cathode materials and a lithium−metal anode. The cycling performance at a rate of 0.1C is depicted in Figure 5a, where batteries with modified solid-state electrolytes demonstrate superior performance, particularly those utilizing PEO + LiDFOB + 5 wt % Al−Li alloy as the electrolyte. After the first few activations, the discharge capacity of the cell containing composite polymer electrolyte with the Al−Li alloy content of 5 wt % did not decay in the following cycling testing. Figure 5b illustrates the rate performance at various current densities. Employing PEO + LiDFOB + 5 wt % Al−Li alloy as the solid-state electrolyte, the initial discharge capacities of the battery at current densities of 0.1, 0.2, 0.5, 1, 2, and 5 C, followed by a return to 0.1C, are 152, 138, 126, 103, 65, 26, and 150 mAh g^{-1}, respectively. The incorporation of varying ratios of Al−Li alloy into the CPEs significantly influences their rate performance. The initial cycle curve, as presented in Figure 5c, indicates that a 5 wt % Al−Li alloy addition to the PEO+LiDFOB matrix yields the optimal initial charge−discharge capacity and is thus considered the most advantageous ratio. Due to the released excess Li^+ from the decomposition of the Al−Li alloy, the initial Coulombic efficiency is higher than 100%. The low polarization voltage observed across all solid-state batteries can be attributed to the enhanced ionic conductivity and improved interfacial contact between the electrolyte and electrodes. Some studies have pointed out that the Li^+ diffusion may be related to the Li trapping effect caused by the repetitive alloy-dealloying processes,[42] but Al−Li alloy in this study will irreversibly decompose and release Li^+ during the initial charge. Therefore, the migration of Li^+ on the ether oxygen group can be accelerated mainly through the interaction between the Al−Li alloy and PEO. Figure S4 shows SEM images of different Al−Li alloy impurities after cycling. Figure S4b shows the transformation of pure PEO from a colorless semitransparent state to a blackened central region, indicating that without the addition of Al−Li alloy filler, pure PEO will deteriorate the contact surface with metallic lithium. During the cycling process, the composite electrolyte film with added Al−Li alloy decomposes to produce Al_4Li_9 alloy,[43,44] which forms a

https://doi.org/10.1021/acsomega.4c05040
ACS Omega 2024, 9, 35920−35928

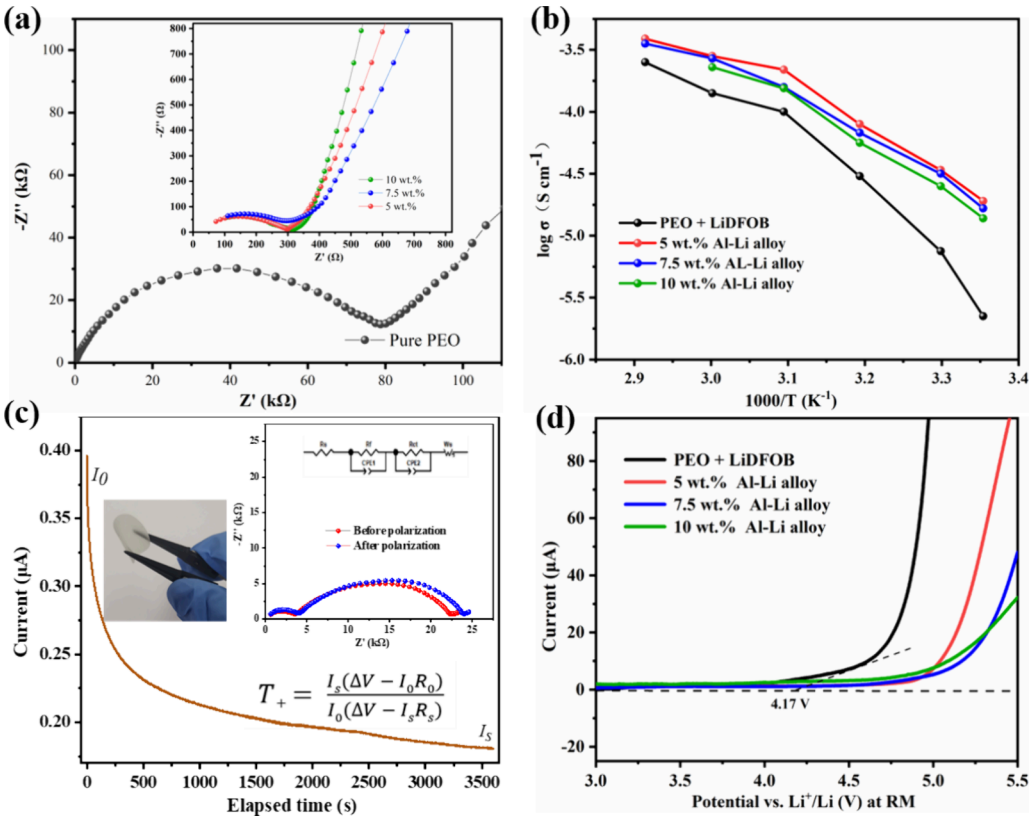

Figure 6. (a) EIS spectra of SS|SPEs|SS symmetrical cells at room temperature. (b) Temperature dependence of the ionic conductivity of the four polymer electrolytes. (c) Chronoamperometry curve of the SS|SPE|SS symmetrical cell based on PEO + LiDFOB at room temperature and its AC impedance spectra before and after the polarization. (d) LSV curves of Li|SPEs|SS cells at room temperature with a scanning rate of 1 mV s^{-1}.

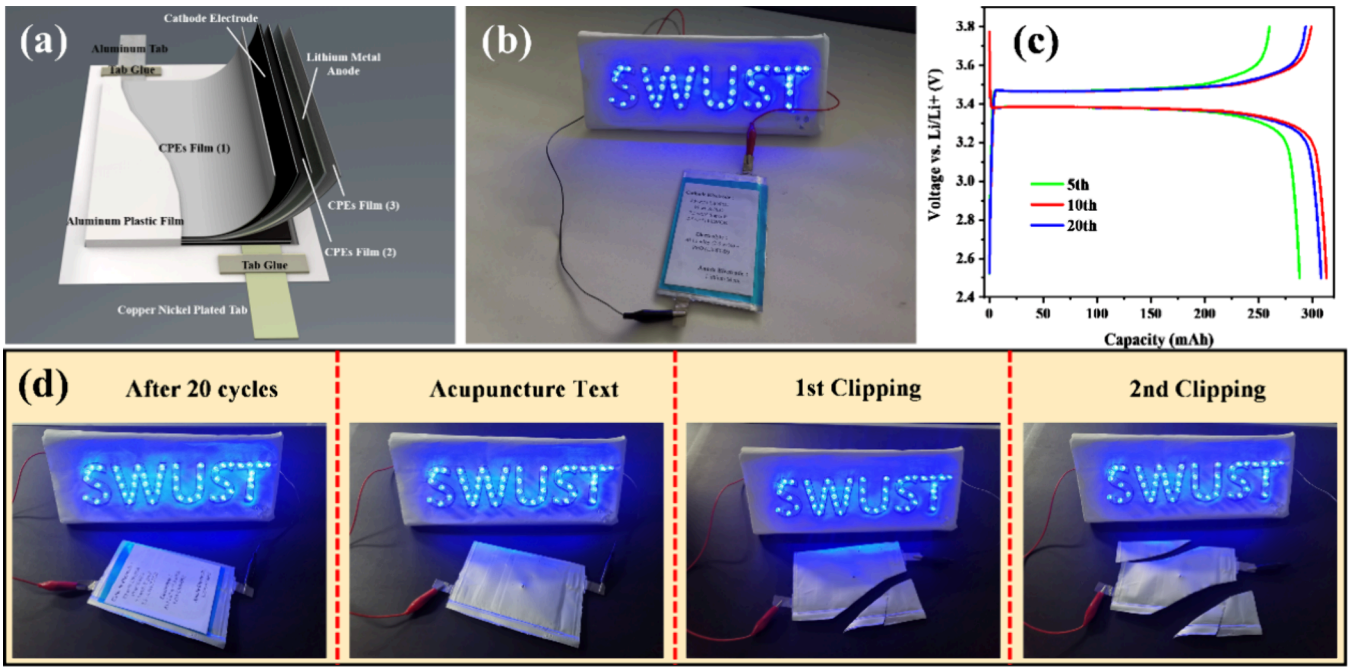

Figure 7. (a) Schematic diagram of the structure of the soft pack battery. (b) Charge−discharge curve of the PEO + LiDFOB + 5% Al Li alloy battery composed of luminous LED lights at 1 C. (d) After 20 cycles of charging, the solid-state pouch cell.

protective layer on the surface of the metallic lithium to avoid deterioration with the lithium metal and suppress the growth and penetration of lithium dendrites. Compared with PEO + LiDFOB + 5 wt % Al−Li alloy, there are more alloy particles dispersed on the surface of the CPEs with higher Al−Li content (7.5 and 10 wt %). When packed with Li metal tightly after the cell assembly, a Li-richer alloy layer (Al_4Li_9) with relatively lower Li^+ diffusivity can be formed in the interface,[40]

https://doi.org/10.1021/acsomega.4c05040
ACS Omega 2024, 9, 35920−35928

driven by potential and Li concentration gradient, which results in poor cycling stability and larger voltage hysteresis of the CPEs with higher Al−Li content.

A series of electrochemical tests were performed on the produced electrolyte membranes. Figure 6a shows a comparison of EIS between PEO + LiDFOB solid electrolyte and the CPEs with variant Al−Li alloy addition. The impedance value of the CPES with the inclusion of the Al−Li alloy is significantly lower than that of PEO + LiDFOB. Figure 6b shows the Arrhenius curve of the composite solid electrolyte. According to the calculation, the ionic conductivity of PEO +LiDFOB and CPEs (with Al−Li alloy addition of 5, 7.5, 10%) is 1.37×10^{-7}, 3.41×10^{-4}, 3.62×10^{-4}, and 3.53×10^{-4} S cm^{-1}, respectively, indicating that the addition of Al−Li alloy can significantly improve the ionic conductivity. Moreover, calculated by the formula shown in Figure 6c, the lithium ionic migration number of PEO + LiDFOB is 0.214. According to Figures S5−S7, the lithium ionic migration numbers of CPEs (with Al−Li alloy addition of 5, 7.5, and 10%) are 0.524, 0.429, and 0.327, respectively. Therefore, the appropriate addition of the Al−Li alloy can increase the lithium ionic migration number, while excessive addition will have the opposite effect. The reasons why Al−Li alloy can increase the lithium ion migration numbers are (1) the alloy will release excess Li^+ during decomposition, increasing the concentration of lithium ions. (2) The ether oxygen group of PEO can provide lone electron pairs and belongs to Lewis bases. The Lewis acid−base interaction between the Al−Li alloy and PEO can promote the dissociation of lithium salts and increase the conduction channels of Li^+.[45] (3) As an active filler, the Al−Li alloy particles can alleviate the crystallization of PEO, so that the ether bond of PEO in the amorphous region rotates with a lower cohesive energy, which is manifested as the chain segment swing at the molecular scale, thereby improving the conduction efficiency of Li^+.[46]

The electrochemical stability of PEO + LiDFOB and CPEs was assessed by using linear sweep voltammetry (LSV). As shown in Figure 6d, the decomposition voltage of PEO + LiDFOB and CPEs (with Al−Li alloy addition of 5, 7.5, and 10%) is 4.17, 4.82, 4.92, and 4.77 V. In short, an appropriate amount of Al−Li alloy addition can reduce impedance and increase the conductivity, lithium-ion migration number, and decomposition voltage of CPEs, thereby improving the electrochemical performance and broadening the voltage window of solid-state batteries.

The structure of a pouch solid-state battery using PEO + LiDFOB + 5 wt % Al−Li is shown in Figure 7a, consisting of cathode electrodes, lithium−metal anode electrodes, and CPE membranes (5 wt % Al−Li addition) stacked on top of each other, without liquid electrolytes and traditional separators. The voltage of the fully charged pouch solid-state battery is higher than 3 V, and it can light up DC LED beads, as shown in Figure 7b. Due to the decomposition of Al−Li alloy providing additional lithium-ions, the initial discharge capacity is higher than the initial charge capacity (Figure 7c), which is consistent with the conclusion from the button-type battery shown in Figure 5c. Al−Li alloy decomposition is basically completed after the first 3 cycles, and the Coulombic efficiency returns to normal, resulting in the stabilization of the pouch solid-state battery's capacity at over 300 mAh. As shown in Figure 7d, after 20 cycles of charging and discharging, even acupuncture and cutting, the solid-state battery not only did not ignite and burn, but also could still light up the LED lamp beads, indicating its excellent safety performance.

4. CONCLUSIONS

A new type of PEO solid electrolyte was synthesized using an aluminum−lithium alloy as a functional filler. This filler plays an important role in electrochemistry, mechanical strength, and excellent compatibility with the lithium metal anode. After the addition of aluminum lithium alloy, PEO + LiDFOB + Al−Li alloy can reduce the crystallinity of polymer chains and provide Lewis acid surface compared to PEO + LiDFO electrolyte, which has higher ion conductivity, larger electrochemical stability window, higher lithium ion transfer number, and better mechanical strength to avoid short circuits. In addition, PEO + LiDFOB + Al Li−5 wt % showed the most excellent improvement in ion conductivity, mechanical properties, and electrochemical performance, demonstrating excellent rate performance and stable cycling performance. Electrochemical analysis shows that this composite electrolyte can not only reduce electrode polarization but also increase the number of lithium-ion transfers. Therefore, this work provides a novel design approach for the future consideration of constructing functional fillers that can increase the migration number of lithium ions to enhance the electrochemical performance of solid-state electrolytes.

■ ASSOCIATED CONTENT

Supporting Information

The Supporting Information is available free of charge at https://pubs.acs.org/doi/10.1021/acsomega.4c05040.

XRD patterns of Al−Li alloys; initial charge/discharge curves of Al−Li alloys; TGA traces of CPEs with various Al−Li alloy content; photographs and SEM images of lithium metal anodes after 100 cycles; chronoamperometry curve of the SS|SPE|SS symmetrical cell based on CPEs with various Al−Li alloy content at room temperature, and its AC impedance spectra before and after the polarization (PDF)

■ AUTHOR INFORMATION

Corresponding Author

Dongyan Ren − *Department of Materials and Construction, Mianyang Vocational and Technical College, Mianyang 621010 Sichuan, China;* orcid.org/0009-0005-9660-9906; Email: 18990178268@189.cn

Authors

Xin Tang − *State Key Laboratory of Environment-Friendly Energy Materials, School of Material and Chemistry, Southwest University of Science and Technology, Mianyang 621010 Sichuan, China*

Qiqiang Wang − *Department of Materials and Construction, Mianyang Vocational and Technical College, Mianyang 621010 Sichuan, China*

Haifeng Du − *Department of Materials and Construction, Mianyang Vocational and Technical College, Mianyang 621010 Sichuan, China*

Ling Ding − *State Key Laboratory of Environment-Friendly Energy Materials, School of Material and Chemistry, Southwest University of Science and Technology, Mianyang 621010 Sichuan, China*

Complete contact information is available at:

https://doi.org/10.1021/acsomega.4c05040
ACS Omega 2024, 9, 35920−35928

https://pubs.acs.org/10.1021/acsomega.4c05040

Author Contributions

[§]D.R. and X.T. are contributed equally to this work.

Notes

The authors declare no competing financial interest.

■ ACKNOWLEDGMENTS

This work was supported by research on recycling application of waste fiber reinforced thermosetting composites (MZ24ZD02).

■ REFERENCES

(1) Bresser, D.; Hosoi, K.; Howell, D.; Li, H.; Zeisel, H.; Amine, K.; Passerini, S. Perspectives of automotive battery R&D in China, Germany, Japan, and the USA. *J. Power Sources* **2018**, *2018* (382), 176−178.

(2) Huo, S.; Sheng, L.; Xue, W.; Wang, L.; Xu, H.; Zhang, H.; Su, Ben; Lyu, M.; He, X. Challenges of Stable Ion Pathways in Cathode Electrode for Al-Solid-State Lithium Batteries: A Review. *Adv. Energy Mater.* **2023**, *13* (15), No. 2204343.

(3) Liu, Q.; Wang, L.; He, X. Toward practical solid-state polymer lithium batteries by in situ polymerization process: a review. *Adv. Energy Mater.* **2023**, *13* (30), No. 2300798.

(4) Feng, W.; Zhao, Y.; Xia, Y. Solid Interfaces for the Garnet Electrolytes. *Adv. Mater.* **2024**, *36* (15), No. 2306111.

(5) Mu, T.; Lu, H.; Ren, Y.; Wan, X.; Xu, X.; Tan, S.; Ma, Y.; Yin, G. Interface defect chemistry enables dendrite-free lithium metal anodes. *Chem. Eng. J.* **2022**, *437*, No. 135109.

(6) Fan, L. Z.; He, H.; Nan, C. W. Tailoring inorganic−polymer composites for the mass production of solid-state batteries. *Nat. Rev. Mater.* **2021**, *6* (11), 1003−1019.

(7) Liu, J.; Bao, Z.; Cui, Y.; Dufek, E. J.; Goodenough, J. B.; Khalifah, P.; Li, Q.; Liaw, B. Y.; Liu, P.; Manthiram, A.; Meng, Y. S.; Subramanian, V. R.; Toney, M. F.; Viswanathan, V. V.; Whittingham, M. S.; Xiao, J.; Xu, W.; Yang, J.; Yang, X. Q.; G, J. Pathways for practical high-energy long-cycling lithium metal batteries. *Nat. Energy* **2019**, *4* (3), 180−186.

(8) Manthiram, A.; Yu, X.; Wang, S. Lithium battery chemistries enabled by solid-state electrolytes. *Nat. Rev. Mater.* **2017**, *2* (4), No. 16103.

(9) Cui, Z.; Hassoun, J.; Tominaga, Y. Development of polycarbonate-based electrolytes with in situ polymerized electrolyte interlayers for lithium-metal batteries. *J. Energy Storage* **2024**, *79*, No. 110175.

(10) Bi, Z.; Sun, Q.; Jia, M.; Zuo, M.; Zhao, N.; Guo, X. Molten salt driven conversion reaction enabling lithiophilic and air-stable garnet surface for solid-state lithium batteries. *Adv. Funct. Mater.* **2022**, *32* (52), No. 2208751.

(11) Huang, C.; Wang, F.; Huang, S.; Hong, J.; Yuan, S.; Hou, S.; Jin, H. The electrochemical failure mechanism investigation of $Li_{1+x}Al_xTi_{2-x}(PO_4)_3$ solid-state electrolytes. *J. Mater. Chem. A* **2023**, *11* (23), 12034−12042.

(12) Akimoto, J.; Akao, T.; Kataoka, K. Low-Temperature Fabrication of Bulk-Type All-Solid-State Lithium-Ion Battery Utilizing Nanosized Garnet Solid Electrolytes. *Small* **2023**, *19* (40), No. 2301617.

(13) Wu, M.; Li, M.; Jin, Y.; Chang, X.; Zhao, X.; Gu, Z.; Liu, G.; Yao, X. In situ formed LiF-Li_3N interface layer enables ultra-stable sulfide electrolyte-based all-solid-state lithium batteries. *J. of Energy Chem.* **2023**, *79*, 272−278.

(14) Holmes, S. E.; Liu, F.; Zhang, W.; Sayavong, P.; Oyakhire, S. T.; Cui, Y. Investigating the Cyclability and Stability at the Interfaces of Composite Solid Electrolytes in Li Metal Batteries. *ACS Appl. Mater. Interfaces* **2022**, *14* (48), 53736−53743.

(15) Zhao, Q.; Stalin, S.; Zhao, C. Z.; Archer, L. A. Designing solid-state electrolytes for safe, energy-dense batteries. *Nat. Rev. Mater.* **2020**, *5* (3), 229−252.

(16) Kuang, J.; Li, X.; Li, Y.; Zhong, Y.; Gu, C.; Xia, X.; Wang, X.; Tu, J. Robust polymer electrolyte with enhanced ionic conductivity realized by the incorporation of electrospun $MgAl_2O_4$ nanofibers. *J. Solid State Electr* **2023**, *27* (12), 3315−3324.

(17) Yang, L.; Zhang, H.; Xia, E.; Wu, Y.; Li, Z. PEO/Li_2ZrO_3 composite electrolyte for solid-state rechargeable lithium battery. *J. Energy Storage* **2023**, *65*, No. 107283.

(18) Wang, X.; Hua, H.; Li, J.; Shen, X.; Zhao, J.; Xie, X.; Zhang, P. Oxygen vacancies on surface of the TiO_2 fillers hinder Li^+ conduction in PEO all-solid-state electrolyte. *Ionics* **2022**, *28*, 85−97.

(19) Masoud, E. M.; El-Bellihi, A. A.; Bayoumy, W. A.; Mousa, M. A. Effect of $LiAlO_2$ nanoparticle filler concentration on the electrical properties of PEO−$LiClO_4$ composite. *Mater. Res. Bull.* **2013**, *48* (3), 1148−1154.

(20) Zheng, Y.; Guo, J.; Ning, D.; Huang, Y.; Lei, W.; Li, J.; Li, J.; Schuck, G.; Shen, J.; Guo, Y.; Zhang, Q.; Tian, H.; Lan, H.; Shao, H. Design of metal-organic frameworks for improving pseudo-solid-state magnesium-ion electrolytes: Open metal sites, isoreticular expansion, and framework topology. *J. Mater. Sci. Technol.* **2023**, *144*, 15−27.

(21) Wang, T.; Liu, X.; Xie, L.; Ji, H.; Wang, L.; Niu, X.; Gao, J. 3D nanofiber framework based on polyacrylonitrile and siloxane-modified $Li_{6.4}La_3Zr_{14}Ta_{0.6}O_{12}$ reinforced poly (ethylene oxide)-based composite solid electrolyte for lithium batteries. *J. Alloys Compd.* **2023**, *945*, No. 168877.

(22) Yan, C.; Zhu, P.; Jia, H.; Du, Z.; Zhu, J.; Orenstein, R.; Cheng, H.; Wu, N.; Dirican, M.; Zhang, X. Garnet-rich composite solid electrolytes for dendrite-free, high-rate, solid-state lithium-metal batteries. *Energy Storage Mater.* **2020**, *26*, 448−456.

(23) Jiang, C.; Zhang, J.; Luo, P.; Yang, Jun; Feng, X.; Zheng, Y.; Shen, Y.; Li, X.; Yang, Z.; Huang, R. Designing an Al-Rich in Situ Coating for Stabilizing High-Energy-Density Li Metal Battery Electrodes via Electrolyte Modulation. *ACS Appl. Energy Mater.* **2023**, *6* (6), 3452−3459.

(24) Wang, C.; Yang, T.; Zhang, W.; Huang, H.; Gan, Y.; Xia, Y.; He, X.; Zhang, J. Hydrogen bonding enhanced SiO_2/PEO composite electrolytes for solid-state lithium batteries. *J. Mater. Chem. A* **2022**, *10* (7), 3400−3408.

(25) Utomo, N. W.; Deng, Y.; Zhao, Q.; Liu, X.; Archer, L. A. Structure and evolution of quasi-solid-state hybrid electrolytes formed inside electrochemical cells. *Adv. Mater.* **2022**, *34* (32), No. 2110333.

(26) Xu, L.; Feng, T.; Huang, J.; Hu, Y.; Zhang, L.; Luo, L. Structural Heterogeneity Induced Li Dendrite Growth in $Li_{0.33}La_{0.56}TiO_3$ Solid-State Electrolytes. *ACS Appl. Energy Mater.* **2022**, *5* (3), 3741−3747.

(27) Mertens, A.; Yu, S.; Schön, N.; Gunduz, D. C.; Tempel, H.; Schierholz, R.; Hausen, F.; Kungl, H.; Granwehr, J.; Eichel, R. Superionic bulk conductivity in $Li_{1.3}Al_{0.3}Ti_{1.7}(PO_4)_3$ solid electrolyte. *Solid State Ionics* **2017**, *309*, 180−186.

(28) Wu, Z.; Wu, Z.; Wang, Z.; Peng, Y.; Li, Z.; Huang, Z.; Mei, W.; Liu, D.; Li, M.; Zhou, W.; Fei, Gao; Cheng, Z.; Luo, G. Effect of Bi_2O_3 on the ion migration and interfacial properties of $Li_{0.33}La_{0.557}TiO_3$ solid electrolytes. *Corros. Sci.* **2023**, *224*, No. 111473.

(29) Case, D.; McSloy, A. J.; Sharpe, R.; Yeandel, S. R.; Bartlett, T.; Cookson, J.; Dashjav, E.; Tietz, F.; Kumar, C. M. N.; Goddard, P. Structure and ion transport of lithium-rich $Li_{1+x}Al_xTi_{2-x}(PO_4)_3$ with $0.3 < x < 0.5$: A combined computational and experimental study. *Solid State Ionics* **2020**, *346*, No. 115192.

(30) Zhu, L.; Zhu, P.; Fang, Q.; Jing, M.; Shen, X.; Yang, L. A novel solid PEO/LLTO-nanowires polymer composite electrolyte for solid-state lithium-ion battery. *Electrochim. Acta* **2018**, *292*, 718−726.

(31) Wang, Q.; Liu, L.; Zhao, B.; Zhang, L.; Xiao, X.; Yan, H.; Xu, G.; Ma, L.; Liu, Y. Transport and interface characteristics of Te-doped NASICON solid electrolyte $Li_{1.3}Al_{0.3}Ti_{1.7}(PO_4)_3$. *Electrochim. Acta* **2021**, *399*, No. 139367.

(32) Wang, X.; Zhang, Y.; Zhang, X.; Liu, T.; Lin, Y. H.; Li, L.; Shen, Y.; Nan, C. W. Lithium-salt-rich PEO/$Li_{0.3}La_{0.557}TiO_3$ interpenetrat-

https://doi.org/10.1021/acsomega.4c05040
ACS Omega 2024, 9, 35920−35928

ing composite electrolyte with three-dimensional ceramic nano-backbone for all-solid-state lithium-ion batteries. *ACS appl. mater. Interfaces* **2018**, *10* (29), 24791−24798.
(33) Chen, Q.; Pan, P.; Zhang, M.; Hu, Y.; Fu, K. A Three-Dimensional Fiber-Network-Reinforced Composite Solid-State Electrolyte from Waste Acrylic Fibers for Flexible All-Solid-State Lithium Metal Batteries. *ACS appl. mater. Interfaces* **2023**, *15* (32), 38507−38521.
(34) Yan, C.; Zhu, P.; Jia, H.; Du, Z.; Zhu, J.; Orestein, R.; Cheng, H.; Wu, N.; Dirican, M.; Zhang, X. Garnet-rich composite solid electrolytes for dendrite-free, high-rate, solid-state lithium-metal batteries. *Energy Storage Mater.* **2020**, *26*, 448−456.
(35) Yin, S.; Huang, Y.; Han, J.; Wang, Y.; Xu, Y.; Seidi, F.; Xiao, H. Cellulosic all-solid-state electrolyte for lithium batteries fabricated via bio-synthetic avenue. *Compos Part B-Eng.* **2023**, *254*, No. 110566.
(36) Palmer, M. J.; Kalnaus, S.; Dixit, M. B.; Westover, A. S.; Hatzell, K. B.; Dudeny, N. J.; Chen, X. C. A three-dimensional interconnected polymer/ceramic composite as a thin film solid electrolyte. *Energy Storage Mater.* **2020**, *26*, 242−249.
(37) Yin, S.; Huang, Y.; Liu, Y.; Cheng, L.; Chen, M.; Xu, Y.; Seidi, F.; XIao, H. Advanced Composite Solid Electrolyte Architecture Constructed with Amino-Modified Cellulose and Carbon Nitride via Biosynthetic Avenue. *Adv. Funct. Mater.* **2024**, *34*, No. 2314976.
(38) Li, X.; Wang, D.; Wang, H.; Yan, H.; Gong, Z.; Yang, Y. Poly (ethylene oxide)−$Li_{10}SnP_2S_{12}$ composite polymer electrolyte enables high-performance all-solid-state lithium sulfur battery. *ACS Appl. Mater. Interfaces* **2019**, *11* (25), 22745−22753.
(39) Zheng, T.; Zhang, J.; Jin, W.; Boles, S.; T. Utilization of Li-rich phases in aluminum anodes for improved cycling performance through strategic thermal control. *ACS Appl. Energy Mater.* **2023**, *6* (3), 1845−1852.
(40) (a) Zhang, J.; Zheng, T.; Lam, K.; Boles, S. T. Design considerations and cycling guidance for aluminum foil anodes in lithium-ion rechargeable cells. *Electrochim. Acta* **2023**, *456*, No. 142437. (b) Teng, J.; Tang, X.; Li, H.; Wu, Q.; Zhao, D.; Li, J. Al-Li alloys as bifunctional sacrificial lithium sources for prelithiation of high-energy-density Li-ion batteries. *J. Power Sources* **2022**, *540*, No. 231642.
(41) Luo, H.; Wang, Z.; Zhao, S.; Fang, Shan; Tian, B.; Ao, X. Dendrite-free lithium anode enabled by lithium atom preferred orientation on AlLi alloy. *Solid State Ionics* **2023**, *402*, No. 116360.
(42) Crowley, P. J.; Scanlan, K. P.; Manthiram, A. Diffusional lithium trapping as a failure mechanism of aluminum foil anodes in lithium-ion batteries. *J. Power Sources* **2022**, *546*, No. 231973.
(43) Chen, S.; Yang, X.; Zhang, J.; Ma, J.; Meng, Y.; Tao, K.; Li, F.; Geng, J. Aluminum-lithium alloy as a stable and reversible anode for lithium batteries. *Electrochim. Acta* **2021**, *368*, No. 137626.
(44) Sun, J.; Zeng, R.; Lv, W.; Yang, Q. H.; Amal, R.; Wang, D. W. A Li-ion sulfur full cell with ambient resistant Al-Li alloy anode. *Energy Storage Mater.* **2018**, *15*, 209−217.
(45) Zhou, Q.; Ma, J.; Dong, S.; Li, X.; Cui, G. Intermolecular chemistry in solid polymer electrolytes for high-energy-density lithium batteries. *Adv. Mater.* **2019**, *31* (50), No. 1902029.
(46) Zhu, X.; Wang, K.; Xu, Y.; Zhang, G.; Li, S.; Li, C.; Zhang, X.; Sun, X.; Ge, X.; Ma, Y. Strategies to boost ionic conductivity and interface compatibility of inorganic-organic solid composite electrolytes. *Energy Storage Mater.* **2021**, *36*, 291−308.

https://doi.org/10.1021/acsomega.4c05040
ACS Omega 2024, 9, 35920−35928